

PAPER • OPEN ACCESS

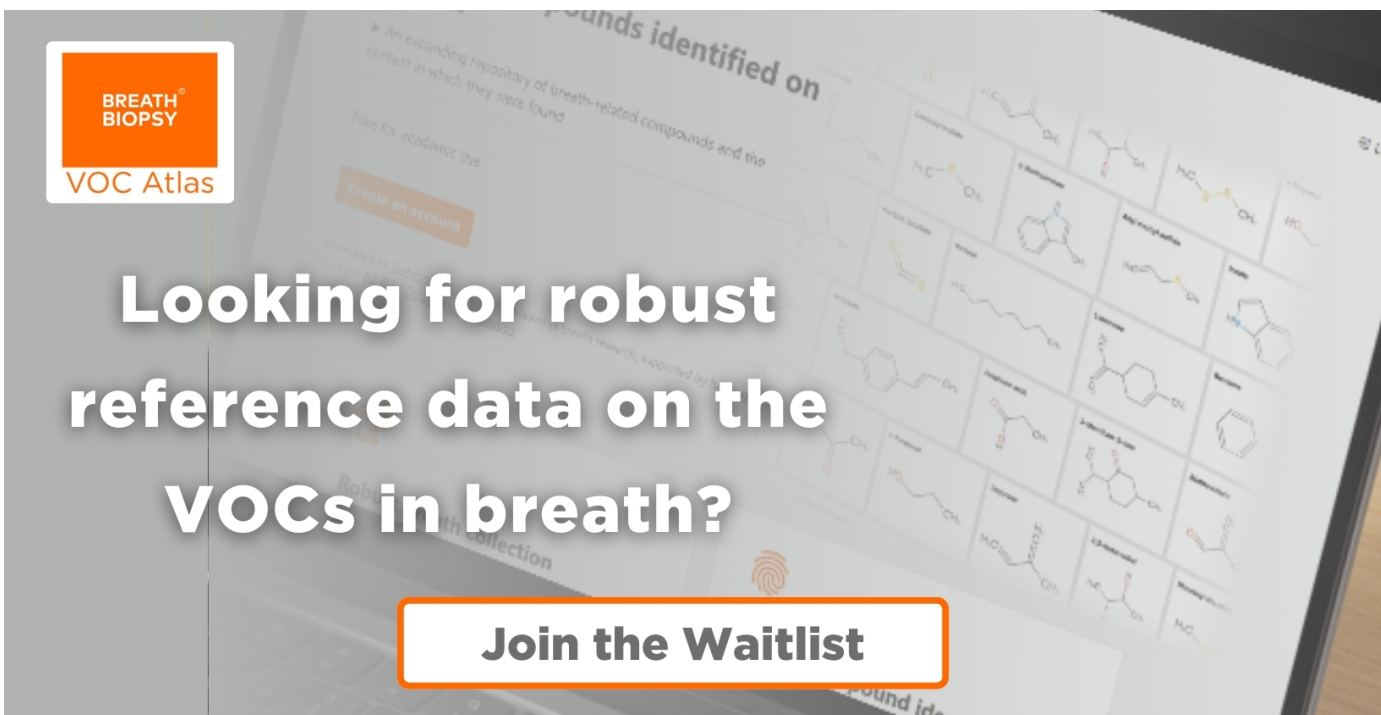
Coupling of photovoltaics with neurostimulation electrodes—optical to electrolytic transduction

To cite this article: Marie Jakešová *et al* 2024 *J. Neural Eng.* **21** 046003

View the [article online](#) for updates and enhancements.

You may also like

- [Flow-induced synthesis of polystyrene–block–poly\(ethylene glycol\) vesicles on the interface of a laminated microflow](#)
Xuan Don Nguyen, Hyeong Jin Jeon, Dong Hyeok Park *et al.*
- [Optical study of thin-film photovoltaic cells with apparent optical path length](#)
Changsoon Cho, Seonju Jeong and Jung-Yong Lee
- [Improving image quality for digital breast tomosynthesis: an automated detection and diffusion-based method for metal artifact reduction](#)
Yao Lu, Heang-Ping Chan, Jun Wei *et al.*



BREATH BIOPSY
VOC Atlas

An expanding repository of breath-related compounds and the context in which they are found

Free for academic use

Create an account

Looking for robust reference data on the VOCs in breath?

Join the Waitlist

170+
Compounds

100+
Diseases

500+
Literature Associations



PAPER

OPEN ACCESS

Coupling of photovoltaics with neurostimulation electrodes—optical to electrolytic transduction

RECEIVED
6 February 2024REVISED
9 June 2024ACCEPTED FOR PUBLICATION
17 June 2024PUBLISHED
2 July 2024

Original content from this work may be used under the terms of the [Creative Commons Attribution 4.0 licence](#).

Any further distribution of this work must maintain attribution to the author(s) and the title of the work, journal citation and DOI.

Marie Jakešová¹, Ondřej Kunovský¹, Imrich Gablech¹ , Dion Khodagholy², Jennifer Gelinás^{3,4} and Eric Daniel Głowacki^{1,*} ¹ Bioelectronics Materials and Devices Laboratory, Central European Institute of Technology CEITEC, Brno University of Technology, Purkyňova 123, 61200 Brno, Czech Republic² Department of Electrical Engineering, Columbia University, New York, NY 10027, United States of America³ Department of Biomedical Engineering, Columbia University, New York, NY 10027, United States of America⁴ Department of Neurology, Columbia University, New York, NY 10032, United States of America

* Author to whom any correspondence should be addressed.

E-mail: glowacki@vutbr.cz**Keywords:** bioelectronics, neurostimulation, photovoltaics, wireless power transfer, microelectrodes**Abstract**

Objective. The wireless transfer of power for driving implantable neural stimulation devices has garnered significant attention in the bioelectronics field. This study explores the potential of photovoltaic (PV) power transfer, utilizing tissue-penetrating deep-red light—a novel and promising approach that has received less attention compared to traditional induction or ultrasound techniques. Our objective is to critically assess key parameters for directly powering neurostimulation electrodes with PVs, converting light impulses into neurostimulation currents. **Approach.** We systematically investigate varying PV cell size, optional series configurations, and coupling with microelectrodes fabricated from a range of materials such as Pt, TiN, IrO_x, Ti, W, PtO_x, Au, or poly(3,4 ethylenedioxythiophene):poly(styrene sulfonate). Additionally, two types of PVs, ultrathin organic PVs and monocrystalline silicon PVs, are compared. These combinations are employed to drive pairs of electrodes with different sizes and impedances. The readout method involves measuring electrolytic current using a straightforward amplifier circuit. **Main results.** Optimal PV selection is crucial, necessitating sufficiently large PV cells to generate the desired photocurrent. Arranging PVs in series is essential to produce the appropriate voltage for driving current across electrode/electrolyte impedances. By carefully choosing the PV arrangement and electrode type, it becomes possible to emulate electrical stimulation protocols in terms of charge and frequency. An important consideration is whether the circuit is photovoltage-limited or photocurrent-limited. High charge-injection capacity electrodes made from pseudo-faradaic materials impose a photocurrent limit, while more capacitive materials like Pt are photovoltage-limited. Although organic PVs exhibit lower efficiency than silicon PVs, in many practical scenarios, stimulation current is primarily limited by the electrodes rather than the PV driver, leading to potential parity between the two types. **Significance.** This study provides a foundational guide for designing a PV-powered neurostimulation circuit. The insights gained are applicable to both *in vitro* and *in vivo* applications, offering a resource to the neural engineering community.

1. Introduction

1.1. Background on implantable photovoltaics (PVs) in the context of wireless power transmission methods

Implantable neurostimulation devices are a ubiquitous tool for *in vivo* neuroscience research and a critical component in bioelectronic medicine [1–3]. In all these applications, miniaturization and wireless powering are in high demand [4–6]. This is important to make next-generation bioelectronics medicine devices surgically less invasive. Moreover, for basic research using small animal models, device footprint is often a serious limitation, therefore finding efficient ways to accomplish wireless electrical neurostimulation can also translate to novel research experiments in neuroscience [7]. Many electromagnetic induction protocols exist to wirelessly transmit power to implantable devices [5, 8, 9]. These solutions, however, suffer from low power transfer efficiency and geometric size/position constraints of both sending and receiving antennas. At least some level of analog circuitry is always necessary on the receiver side to convert the incoming electromagnetic signal into a charge-balanced, biphasic electrical stimulation pulse. Therefore, the device must consist, at minimum, of receiving coil, electronic circuit components like rectifiers, and finally the stimulation electrodes interfaced with the target tissue. A promising alternative technique is ultrasound power transfer, which, per unit area, often represents a more efficient alternative to inductive power transfer, but with the necessity of close contact of the transmitter on the surface of the skin [10, 11]. These devices require a piezoelectric transducer to convert acoustic energy into electrical signals. Unfortunately, most of the efficient piezoelectric materials are toxic compounds, creating a barrier to practical adoption. A combination of resonant magnetic power transfer and piezoelectrics is the magnetoelectric power transfer concept elaborated by Singer *et al* [12]. These approaches show an impressive shrinking of device footprint, nevertheless the piezoelectric material remains an issue, and relatively large and inefficient transmitting coils must be used. Optical power transfer using light wavelengths in the tissue transparency window represents an emerging concept which has been explored relatively less than inductive or ultrasound power transfer. This is likely because intuitively anyone can observe that most biological tissues are highly opaque due to absorption and scattering. However, there are regions of the visible and near-infrared spectrum where local maxima for light transmittance exist. These are sometimes referred to as tissue transparency windows, where absorption from biomolecules is largely absent, and scattering is also minimized. The first ‘window’ is between roughly 630–900 nm, and the second is between 1000 and 1350 nm [13, 14]. Wavelengths in these regions can

penetrate into tissue to some degree. Several examples of implantable PVs have been shown to effectively and safely operate at depths of a few mm below the skin, even down to around 10 mm, with red or infrared light being delivered from outside of the body [15, 16]. Since PVs are diodes, the simple connection of a PV to two electrodes shorted by an electrolyte already acts as a rectifier circuit that will transduce a square pulse of light (basically light on/off), into a biphasic current pulse with a high degree of charge balance just from the nature of this simple circuit [17, 18]. If the stimulation electrodes are integrated directly onto the PV itself as thin-films, this represents a very simple and compact system with competitive charge per unit area (or per unit volume) that exceeds the aforementioned technologies [16]. The concept of PV neurostimulation has been deployed in various ways over the past two decades. The most prominent are examples of PV devices for optoelectronic stimulation of the retina, which must be seen as a special use case. Here, light ingress is trivial due to the pupil, and red/infrared light is not absolutely required [19–21]. In these applications, a focused light beam is used to actuate a PV pixel which in turn locally stimulates the retina. The low scattering in the eye vitreous allows laser excitation to be highly collimated and thus it is possible to raster scan across an implant to produce spatially-precise stimulation. These devices comprise a PV cell connected to a primary and return stimulation electrode. In the system reported by Palanker *et al*, silicon PV cells (a series of 2 or 3 to increase the voltage) are monolithically integrated with stimulation/return microelectrodes [19, 22, 23]. These PV stimulators have been tested in animal experiments and there are promising results from clinical trials [24]. Ghezzi *et al* [20, 25] and Rand *et al* [17] have reported organic PV analogs, successfully testing these devices *in vitro* and *in vivo*.

While the eye presents a kind of ‘ideal’ scenario for precise light-based stimulation, every other kind of implantable target (i.e. brain, peripheral nerve) involves transcutaneous operation and will be faced with higher loss of transmitted light power, and also light scattering in the intervening tissues. This fact necessitates the use of wavelengths in the red/near infrared region, to more effectively penetrate hard and soft tissues. Thin-conformable PVs have been shown to operate as cortical stimulators, actuated transcranially in mice [26], and several examples of transdermal PV stimulators have been published [27], operating down to a depth of roughly 1 cm. There have been recent reports of using PV arrays to recharge implantable pacemaker devices, even via harvesting ambient light [28, 29]. There are two approaches to reach deeper stimulation targets. The first is to create leads between the stimulation electrodes and the PV, which can be implanted in a shallower region closer to the skin interface [30]. The

second is to use implantable fiber optics to channel the light to the region of interest [15].

1.2. Semiconductor materials for implantable PVs

Three categories of light-absorbing semiconductor materials have been explored for implantable PVs: Silicon, inorganic compound semiconductors, and organic semiconductors. The distinctions between these different PV types are important, as each approach has advantages and disadvantages that will affect which type of PV is the best for a given application. The basic figures of merit to consider are power conversion efficiency and quantum efficiency. Silicon PVs have 2–10 times higher power conversion efficiency and quantum efficiency than OPVs, depending on the particular organic or silicon device considered. Meanwhile, optimized compound inorganics like GaAs can have even higher power conversion and quantum efficiency numbers, higher than silicon by several percent. In terms of efficiency, GaAs > Si >> Organics. The next consideration is absorption coefficient, which will dictate the practical thickness of the semiconductor layer to efficiently absorb light. Organic semiconductors typically excel in this category, having absorption coefficients over an order of magnitude higher than Silicon, and on par or slightly higher than the best inorganic compound materials. Therefore, if minimization of thickness and volume is important for a given application, compound semiconductors or organics will outperform silicon. Silicon approaches benefit from a mature and highly-accessible microfabrication pathway, and the opportunity to use different commercial silicon wafers or thin-film silicon from chemical vapor deposition methods. The main drawbacks of silicon are mechanical rigidity, low optical absorption coefficient, and necessity of high-quality passivation to prevent surface recombination losses and thus photovoltage drops. Finally, there is the issue of stability. Silicon needs careful passivation and encapsulation to remain stable to corrosion in physiological environment [31]. On the other hand, this can be an advantage. Silicon can dissolve in the body in a relatively harmless way, prompting demonstrations of transient, dissolvable, implantable power sources [31]. Recently, the group of Bozhi Tian has published a high-performance and versatile silicon platform of this type [32]. OPVs suffer from lower efficiency, yet can be made extremely thin (sub-100 nm), on account of the high absorbance coefficient, and are intrinsically mechanically soft and flexible. Compatibility with thin-film polymeric substrates like parylene-c or polyimide is ensured by low-temperature processibility of OPVs. Moreover, some organic semiconductors appear to be very stable in direct contact with physiological medium, without any passivation. Thus, for applications where conformal application is desired, such as a nerve cuff or cortical surface electrode, thin and flexible

devices based on organic semiconductors can be favorable. While compound inorganic semiconductors can be very thin and of highest performance, they present processing difficulties. GaAs and its derivatives are produced via specialized and expensive epitaxial deposition processes requiring toxic gases and high temperatures. The presence of potentially toxic arsenic is a barrier to adoption, though it has been reported that leeching of arsenic from the implant is within safe limits [33]. To-date, the smallest-footprint devices in terms of volume and thickness are made of GaAs [15] or organic semiconductors [16, 34]. In terms of optimized high-performance compound inorganic PV stacks, Sahin and colleagues have published a series of papers on floating light activated micro-electrical stimulators (FLAMESs), comprising optimized heterojunctions of GaAs, giving photovoltage up to 0.7 V [15, 35, 36]. The FLAMES devices were on the size order of several hundred micrometers, and could achieve wireless intraspinal stimulation in the rat spinal cord. Larger arrays of GaAs cells were recently demonstrated in a transdermal power transfer system for wireless powering of implantable electronics. Here, series and parallel connections were used to give a max of 2.4 V and overall several microwatts of power [8]. On the OPV side, our research group has reported efficacious organic stimulation devices implanted up to 15 mm below skin and soft tissue/bone for the stimulation of peripheral nerves or the cortical surface [16, 26, 30]. These latter devices are based on the minimalistic organic photocapacitor design, where the PV diode is itself the stimulation electrode, the whole device is ultraflexible and has a thickness of under 5 μm [34]. Ferlauto *et al* have developed flexible and foldable OPV-based stimulators [20], which present a surgical advantage of being implantable through a small incision and then unfolded in the target area. Overall, organic semiconductors have good indications from combined biocompatibility and nontoxicity, while being stable and inert in the body without need of extensive passivation which would be required for inorganic semiconductors. However, the question of long-term reliability and safety of implantable PVs remains an open one that must be rigorously confronted to allow progress in this field.

It is noteworthy that in parallel to PV-driven neurostimulator devices, there is a growing body of research describing micro or nanoparticle interfaces which, when excited by light, can deliver stimulation to cells and tissues with a variety of mechanisms, including often an interplay of photothermal and photoelectric effects [37–45]. Such microscaled materials can form single-cell interfaces. These types of particle-based photostimulation concepts hold great promise in pushing the limits of miniaturization and obtaining the least surgically-invasive solution. Ideas of untethered and injectable particles have been proposed. The various stimulation mechanisms have

been reviewed in detail to some extent for micro/nanoparticles [42, 46–50]. A fraction of the reported particles operate via a PV mechanism. For those that do, the findings discussed in this paper should in principle apply as well. To perform optimal extracellular stimulation, a microparticle should have a cathode and anode component to optimize photocharge density and spatially separate the charges to maximize the resultant electric field. In this way, the device operates according to the measurements laid out in this work.

This work concerns direct PV stimulation, where a PV diode is connected to a stimulation neural interface. To date, the quantity of successful implanted PV stimulation demonstrations is relatively small, and a primary reason is that specialists from the optoelectronics/PV field do not often overlap with the neural interface device field. We seek to bridge this gap and we have performed this study to map and explain the parameters needed when combining a PV driver with neurostimulation electrodes (figure 1(a)). In this work, we have endeavored to give a roadmap for designing PV neurostimulation devices, giving attention to critical parameters: stimulation electrode type, electrode impedance, PV driver type, serial/parallel connections, and optical pulse intensity and frequency. With these details determined, it is possible to design a PV neurostimulation device tailored to a specific application.

1.3. Measuring the PV-driven neurostimulation circuit

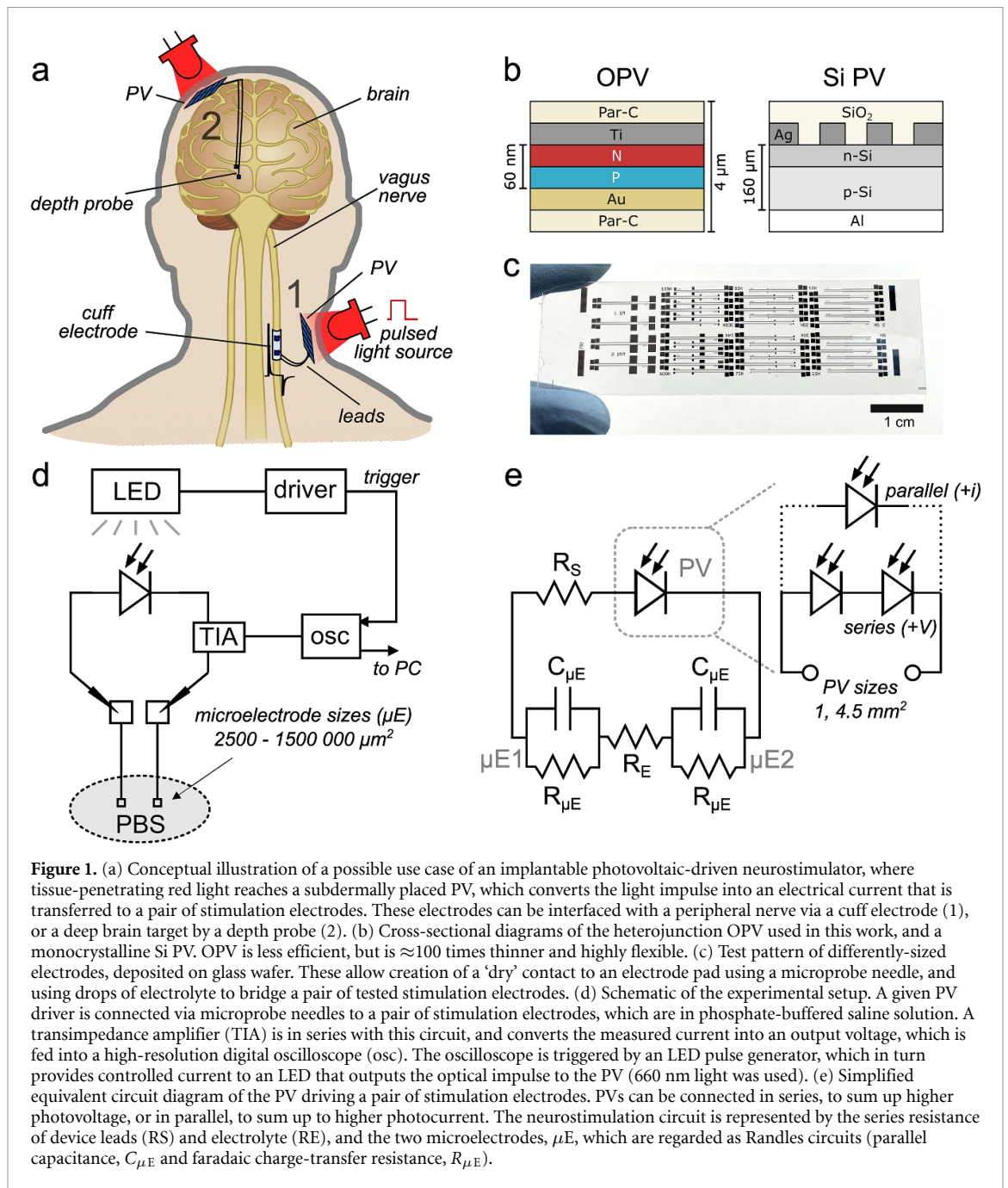
An illuminated PV is a power source, behaving neither as an ideal current nor an ideal voltage source. The current drawn from the PV will depend on the amount of photocurrent generated by the cell, as well as the impedance of the load that is attached to the cell. The maximum photovoltage produced by a single PV is limited by thermodynamics, specifically by the parameter of bandgap of the semiconductor material comprising the cell [51]. Other losses, like charge recombination and series resistance will practically limit cell voltage. Generally, a single-junction Si PV can provide around 0.5 V at open-circuit. OPVs, depending on the materials used, generate between 0.4 and 0.8 V [52]. The OPV tested in this work is made from a heterojunction of phthalocyanine and perylene tetracarboxylic diimide derivatives [53], a combination we have optimized, and which yields an open-circuit voltage of 0.5 V [54]. Therefore, the two PV types compared in this work are essentially equivalent in terms of open-circuit voltage. The OPV and Si PV used in this work are schematized in figure 1(b). We used commercial monocrystalline silicon solar cell wafers, with contact lines and passivation already deposited. These were diced to yield different chip sizes. The OPVs were fabricated at the desired size directly in-house. Arrays of (micro)electrodes were

prepared on glass or silicon wafers, using photolithography techniques (figure 1(c)). The characterization of PV-driven neurostimulation electrodes was performed by connecting the terminals of the PV with a given combination of electrodes which are bridged by electrolyte, and measuring the current that flows through this circuit upon application of a pulse of red light (figure 1(d)). This setup allows evaluation of different permutations of PV drivers with different electrodes. The overall configuration can be regarded as a PV diode short-circuited by a load consisting of two electrolytic contacts and the intervening electrolyte (figure 1(e)). The electrolytic contacts can be understood in terms of the Randles model, of a capacitive component in parallel with a resistive component. The resistive components correspond to faradaic reactions, while the capacitance will be given by the charge injection capacity of the electrode material. An illuminated PV will act as a power source, capable of generating a photovoltage and a photocurrent. The magnitude of current that flows over the whole circuit will depend on the impedance and charge injection capacity of the electrode/electrolyte interfaces. The fundamental limitation of PV neurostimulator approaches is that it is challenging to obtain high driving voltages—a single PN junction, in practice, can rarely produce more than >1 V.

2. Materials and methods

2.1. Fabrication of OPVs

Glass wafers ($500 \pm 20 \mu\text{m}$) were coated with a base layer of $2 \mu\text{m}$ parylene-C grown by CVD (SCS Labcoter PDS 2010). Then, a stack of 1 nm Pd, 9 nm Au, 30 nm Ti, 50 nm Au, 10 nm Ti were deposited via magnetron sputtering (Bestec GmbH). The first photolithography step defined the shape of the PV bottom electrode, anode/cathode leads, and contact pads. AZ 1518 photoresist spin-coated at 4000 rpm was exposed through a soda lime mask using a SÜSS MicroTec MA8 mask aligner equipped with an i-line filter. The resist was developed in AZ 400 K developer diluted 1:4 in deionized water (DI). The metal layers were etched in a KI/I₂ (Au, Pd) and HF/H₂O₂/H₂O (Ti) etch mixtures. The resist was stripped using acetone. Using the same processing, the second photolithography step was used to remove the top Ti/Au/Ti layers to yield a defined, semi-transparent PV bottom electrode area. Next, the organic PN layer was deposited through a shadow mask. Metal free phthalocyanine (H₂Pc, Alfa Aesar) and *N,N'*-dimethyl-3,4,9,10-perylenetetracarboxylic diimide (PTCDI, BASF) were purified by threefold temperature-gradient sublimation. Layers of 40 nm H₂Pc and 50 nm PTCDI were thermally evaporated from resistively heated crucibles (Edwards 306, $<2 \times 10^{-6}$ Torr, rates of 1–6 Å s⁻¹). The OPV top electrode was a 70 nm layer of Ti, which was deposited through a shadow mask using an E-beam evaporator (Bestec GmbH, $<1 \times 10^{-7}$ Torr, at a



rate of 5 \AA s^{-1}). The devices were encapsulated with a $2 \mu\text{m}$ parylene-C layer with 3-(trimethoxysilyl)propyl methacrylate (A-174) present in the CVD chamber as an adhesion promoter. The third photolithography step was used to expose the contact pads. A thicker layer of AZ 1518 was spin coated at 1000 rpm to serve as an etch mask during reactive ion etching (RIE, Oxford Instruments PlasmaPro 80, 200 W, 50 sccm O_2 , 100 mTorr) of the parylene-C layer. The resist was stripped in acetone and the top 10 nm Ti layer was wet etched to expose Au-coated contact pads.

2.2. Fabrication of electrode arrays

Glass or Si wafers with a thermally grown SiO_2 layer ($525 \pm 25 \mu\text{m}$ and $2.6 \mu\text{m}$, respectively) were used as

substrates. In all cases, the electrode area, leads, and contact pads were composed of E-beam evaporated 20 nm of Ti and 50 nm Au (and 30 nm Ti for titanium electrode arrays) deposited onto O_2 plasma activated substrates (Diener NANO Plasma Cleaner). The layout was patterned with AZ 1518 (4000 rpm) and wet etching as specified in OPV fabrication section. Next, the surface was activated by O_2 plasma (Diener) and a $2 \mu\text{m}$ parylene-C encapsulation layer was deposited using the A-174 adhesion promoter. The contact pads were exposed through a thick AZ 1518 (1000 rpm) etch mask using RIE (200 W, 50 sccm O_2 , 100 mTorr). In case of the Au and Ti electrode arrays, the electrode areas were opened directly after using the third lithography mask. All other electrode materials were

patterned by the parylene peel-off technique. For that purpose, an anti-adhesive layer of 2% Micro 90 soap (International Products) was spin coated at 1000 rpm and left to air dry before deposition of the sacrificial 2 μm parylene-C layer. The electrode area was opened through an AZ 12XT (3000 rpm, AZ 326 MIF developer) thick etch mask using RIE (200 W, 50 sccm O_2 , 100 mTorr). The residual resist was stripped in acetone. Before deposition of the electrode material, the substrates were O_2 plasma activated. W was deposited by magnetron sputtering (100 nm, Bestec GmbH), Pt and TiN by ion beam sputtering (100 nm with 5 nm Ti sticking layer, Bestec GmbH) [55], IrO_x and PtO_x by reactive magnetron sputtering (240 nm, [56]). The sacrificial parylene-C was carefully peeled off under DI. The poly(3,4-ethylenedioxythiophene):poly(styrene sulfonate) (PEDOT:PSS) layer was deposited by spin coating. The solution was prepared freshly before deposition and contained PEDOT:PSS (PH1000, Heraeus GmbH), 5 wt% ethylene glycol (EG), 0.1 wt% 4-dodecylbenzenesulfonic acid (DBSA) and 1 wt% (3-glycidyloxypropyl)trimethoxysilane (GOPS). The mixture of PH1000, EG and DBSA was sonicated for 45 min to ensure homogeneity, GOPS was added just before use and sonicated for 2 min. PEDOT:PSS filtered through a 0.45 μm polyvinylidene fluoride membrane filter was spincoated in three layers (3000, 750 and 750 rpm) with a 40 s bake at 90 °C after each layer. After the last coat, the sacrificial parylene-C layer was peeled off yielding the microelectrodes. The wafer was finally annealed at 140 °C for 1 h and then washed in DI to remove the residual soap and other chemicals.

2.3. Preparation of Si PV chips

125 mm \times 125 mm monocrystalline silicon PVs, rated at 2.8 W, were obtained from *CincoSolar* (China). 16 variations of silicon PV cells were prepared by mounting them on alumina ceramic substrates (Elceram, Czech Republic). To achieve interconnection of 1, 2, or 3 series or 2 parallel combinations of silicon PV cells with active surface area of (1.0, 4.5, 25, and 100) mm^2 , alumina substrates with silver leads and pads relying on thick-film technology were employed. The silicon PV cells were originally manufactured with Al metallization that is already partially oxidized upon delivery. Therefore, a hard mask was used to expose only the Al metallization of the chip and RIE was performed to remove aluminum oxides on both sides. Subsequently, 100 nm of Au were evaporated through a shadow mask (Bestec GmbH) to minimize the risk of undesired contact resistance. In the next step, the PV cells were covered with positive photoresist and cut into single chips using a dicing saw (ESEC 8003). The last step of silicon PV

cell fabrication involved removal of the photoresist before mounting on the alumina substrate. Such prepared PV cells were glued to alumina with silver-filled epoxy glue (Epo-tek H21D, Epoxy technology, USA) from the bottom side providing strong mechanical adhesion and low-ohmic electrical contact, while the top side of the PV cells was connected to the Ag pad on alumina using 25 μm Au wire with wedge-wedge thermosonic wire-bonding technique (TPT HB 16).

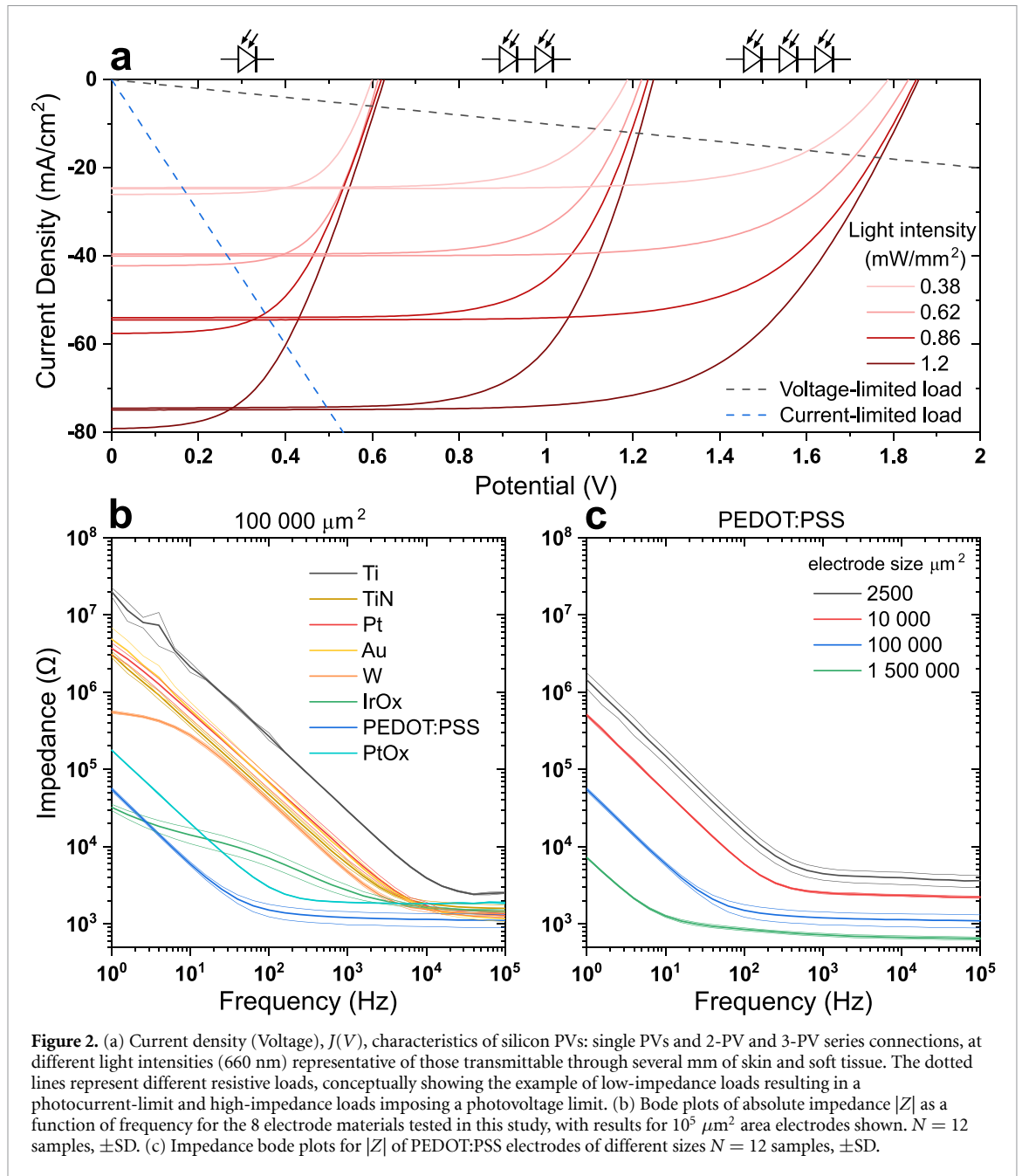
2.4. Electrochemical and optoelectrochemical characterization

The first experiment was focused on electrical impedance spectroscopy measurements of fabricated microelectrodes from Ti, TiN, Pt, Au, W, IrO_x , PEDOT:PSS and PtO_x in a domain of frequencies ranging from 100 kHz to 1 Hz at a voltage amplitude of 10 mV. Our optoelectrical devices were then utilized in custom-made docking station created by 3D printing method from polylactic acid. Alumina with silicon PV cells was glued to the sample holder and inserted into a station equipped with pogo-pins for electrical contact and red LED array for sample irradiation with wavelength of $\approx 656\text{--}660$ nm peak. Intensity was calibrated using a Thorlabs SM1PD1A photodiode. The LED was driven using a Thorlabs DC2200, using the internal pulse generator to trigger the oscilloscope. The functionality of prepared devices was verified via $J(V)$ characteristic measurements in a range from 0 to 2 V at different continuous red light irradiation power densities of (0, 0.38, 0.62, 0.86 and 1.20) mW mm^{-2} . The final experiment was carried out by optoelectrochemical characterisation of PV cells connected to microelectrodes using microprobers. Dynamic measurements of photocurrent were transduced to voltage using a transimpedance amplifier (FEMTO GmbH, DLPCA-200, gain set to 1000) and captured by oscilloscope (Picoscope 4262).

3. Results

3.1. Key characteristics of the PV and stimulation electrodes measured independently

The most common method of PV characterization is a $J(V)$ sweep, where current density (J) is measured while applying different voltages to the cell. Representative $J(V)$ curves for Si PVs are plotted in figure 2(a), showing the dependence on light intensity and the serial connection of 2 and 3 PVs to boost the voltage. $J(V)$ plots can be used as a guide to estimate how much charge a PV can deliver over a given stimulation circuit, and to choose PV size and series arrangement appropriately. High-impedance loads, such as small microelectrodes, will require series connections to provide sufficient photovoltage to deliver

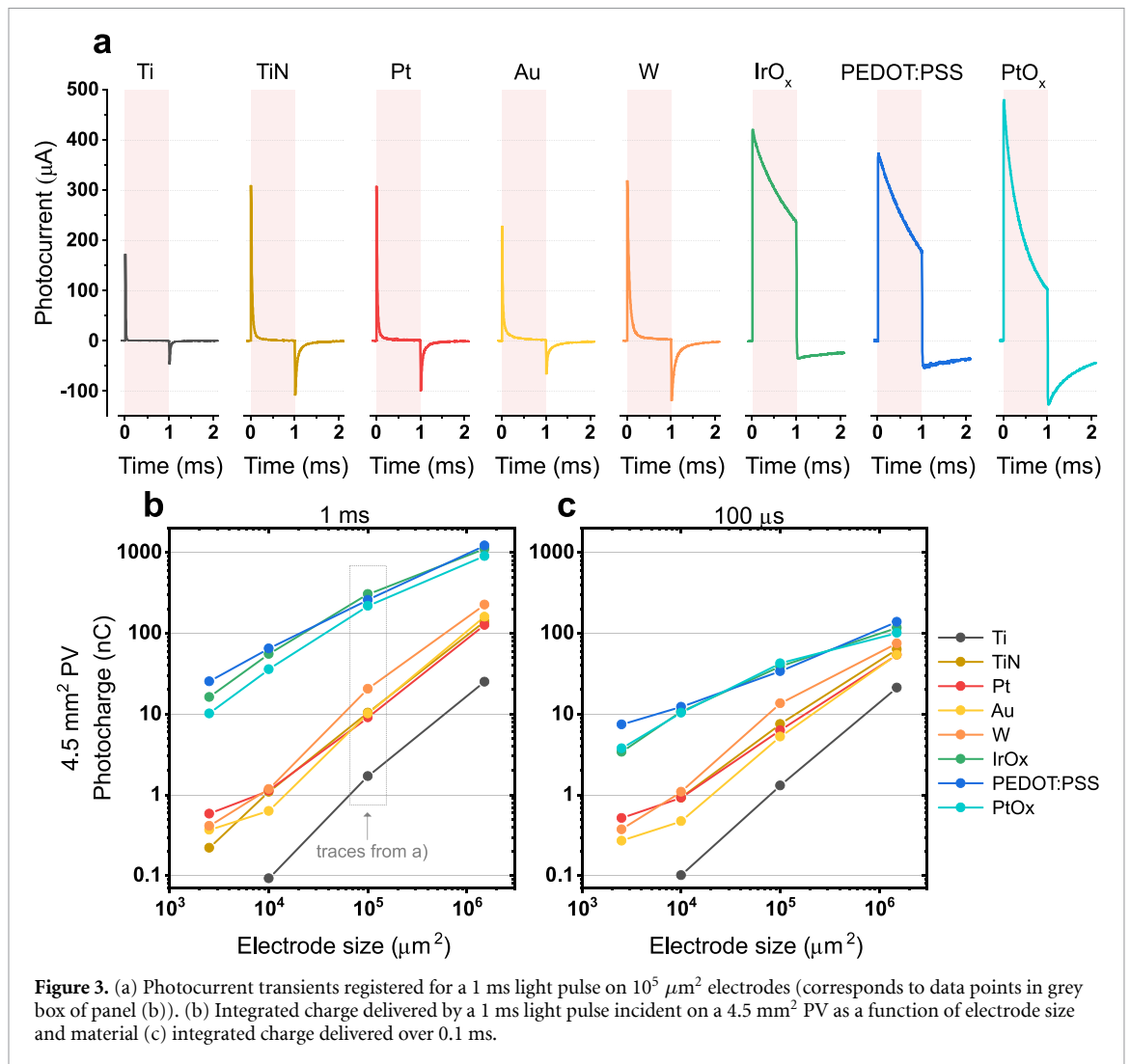


the current/charge necessary for a given neural target. To reproduce practically-relevant scenarios in neural engineering applications, we used eight different neural interface electrode materials, which give a range of impedances and charge injection mechanisms (e.g. capacitive versus faradaic versus pseudo-capacitive). A comparison of absolute impedance values, $|Z|$, as a function of frequency, is shown in figure 2(b). The lowest impedance values are generally provided by the high charge-injection capacity materials PEDOT:PSS, IrO_x, and PtO_x (nanoporous Pt). The former two materials support bulk volumetric capacitance due to highly reversible faradaic reactions, while the latter PtO_x is simply a very high surface-area material. Other materials, like Pt and

TiN which are commonly used in clinical implants, have moderate impedance values. Ti has the highest impedance, due to its native TiO_x layer. Electrode size-dependence impedance plots are shown for the overall best-performing material in terms of low impedance: PEDOT:PSS (figure 2(c)).

3.2. Photocurrent measured from PV + stimulation electrode combinations

Different PV drivers were wired together with stimulation electrode pairs as shown in figure 1(d) and detailed in section 2.4. As a starting point, we consider a single 4.5 mm² Si PV, illuminated with 0.1 or 1 ms impulses of light with an intensity of 1.2 mW mm⁻², and we vary the size of the stimulation electrodes. The



measured current transients and integrated charge are shown in figure 3. Stark differences in current transients occur due to the material type (figure 3(a)). The relatively low voltage afforded by PVs (compared to a typical neurostimulation current isolator that can have compliance voltage of several volts or more) means that for most typical metallic electrode materials (Ti, TiN, Pt, W, Au) the current transients are essentially purely double-layer capacitive, with minimal faradaic component. The pseudo-capacitive materials IrO_x , PEDOT:PSS, and PtO_x , all have high capacitance values and thus can accommodate much more charge at a given voltage. For this reason, the total delivered charges can be 10 times higher for these materials (figure 3(b)). For short pulse times, 0.1 ms, the advantage of the pseudo-capacitive materials is not as great (figure 3(c)). It is clear, however, that for a single PV where the total available driving voltage will not exceed 0.5 V, choosing as low-impedance

electrode materials as possible is critical to building a practical stimulator.

In the next set of presented experiments, we vary Si PV size (1 mm^2 versus 4.5 mm^2) and evaluate the effect of series connection of 2 or 3 cells, as well as a parallel connection of two discrete cells (figure 4). Light intensity and pulse length are held constant. Several clear trends emerge. Adding series connection increases the amount of delivered charge only in the case of voltage-limited circuits, that is those comprising small electrodes and/or higher impedance materials. For materials like PEDOT:PSS, using a double or triple series only helps for electrodes $< 10^4 \mu\text{m}^2$. Larger PV size boosts charge for low-impedance electrodes, whereas if the circuit is voltage-limited increasing the PV size will not result in any more delivered charge. This is critical, as increasing PV device size can be wasteful and only makes sense if impedance of the stimulation circuit is

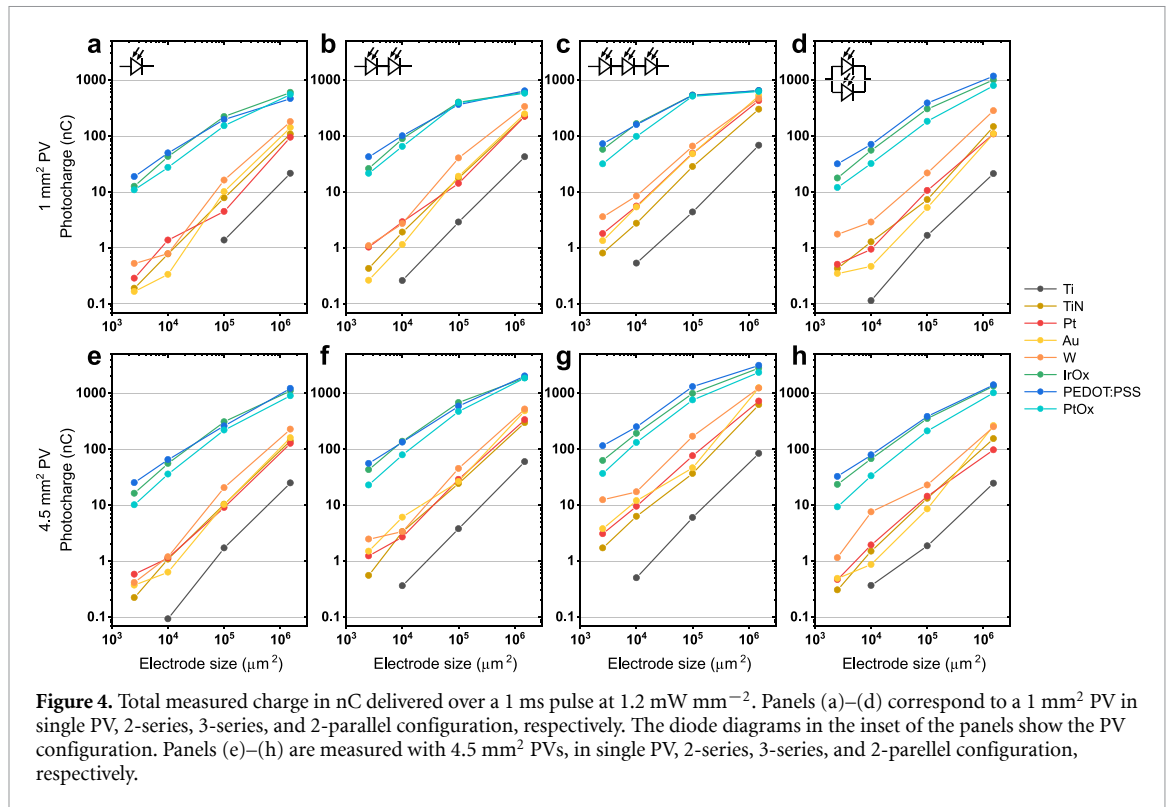
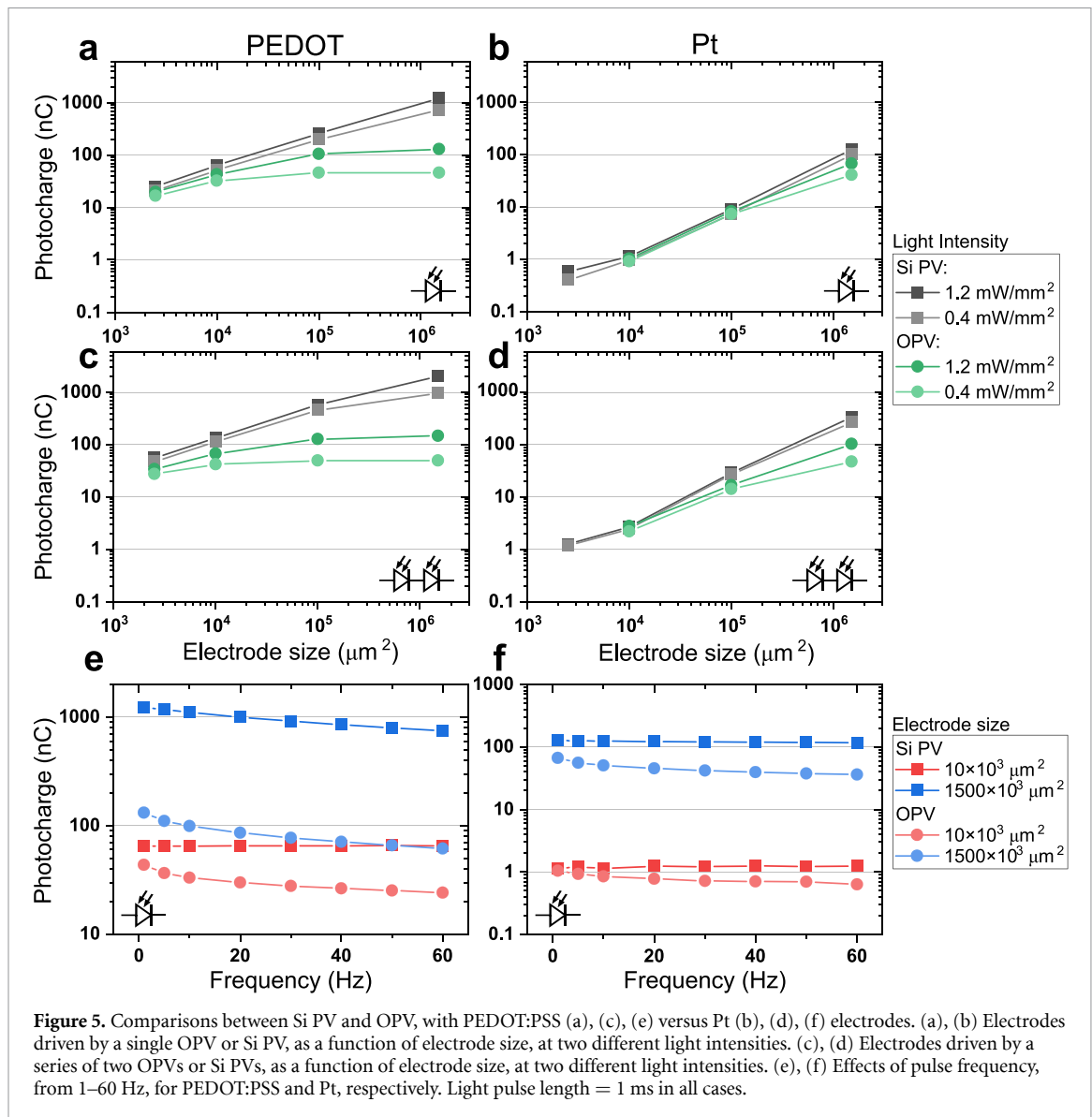


Figure 4. Total measured charge in nC delivered over a 1 ms pulse at 1.2 mW mm^{-2} . Panels (a)–(d) correspond to a 1 mm^2 PV in single PV, 2-series, 3-series, and 2-parallel configuration, respectively. The diode diagrams in the inset of the panels show the PV configuration. Panels (e)–(h) are measured with 4.5 mm^2 PVs, in single PV, 2-series, 3-series, and 2-parallel configuration, respectively.

low enough. This principle also applies when considering conversion efficiency of PVs: higher efficiency may not be of significant benefit if the circuit is photovoltage-limited.

With these principles of photovoltage and photocurrent limitations clearly demonstrated, we next moved to compare Si PVs with OPVs (all PVs had the same area = 4.5 mm^2), as well as the effect of light pulse frequency, using PEDOT:PSS and Pt as two representative electrode materials. Both types of PVs give the same open-circuit voltage. In the case of high-impedance electrodes, (small PEDOT:PSS or all but the largest Pt electrodes) OPV and Si PV deliver the same charge (figures 5(a) and (b)). Adding series connections of either type of PV follows the same general trend as established previously, more charge can be loaded onto higher-impedance electrodes (figures 5(c) and (d)). The advantage provided by the more efficient Si PVs becomes apparent only in cases of large stimulation electrodes, where the total charge will become limited by the photocurrent generation efficiency. We tested pulse frequencies between 1 and 60 Hz (figures 5(e) and (f)). In general, there is always some decline in the charge delivered in each 1 ms pulse as frequency increases. This is due to the issue of PV diodes discharging in the dark between light pulses. If the next pulse arrives before the circuit is fully discharged, the subsequent

total charging voltage will be lower. This effect is mild in Si PV-driven circuits, while in OPV the frequency roll-off in current amplitude is significantly larger. This is caused by the fact that OPVs have very low charge mobility in the dark, therefore the OPVs do not discharge quickly. Si has high mobility and charges can recombine inside the device relatively rapidly, ensuring that the whole circuit can discharge before the next pulse arrives. In case of the larger PEDOT:PSS electrodes, we can also observe a frequency roll-off also with Si PV, as this is imposed by the slow discharge kinetics of the PEDOT:PSS electrode. The issue of discharge kinetics causing frequency roll-off can be resolved by engineering a shunt resistor in parallel with the PV diode, a solution suggested by Palanker *et al* for PV-driven retinal stimulators [19]. Exploring higher-frequency operation ($>1 \text{ kHz}$) may be uniquely relevant in the case of PV stimulators which have an intrinsic voltage limitation. The use of high-frequency pulse trains, where numerous subthreshold-amplitude pulses arrive at the cell in short succession, can result in the summation effect, causing effective depolarization of cell membrane despite the fact that each individual pulse has too low amplitude to depolarize cells [57, 58]. This kind of high-frequency approach has not been used in PV stimulation to our knowledge, but would be interesting to try.



4. Conclusions

PV neurostimulation is a unique approach to wireless modulation of central or peripheral nervous targets. Conceptually, it represents something of a midpoint between conventional implantable microelectrodes and fully noninvasive electrical stimulation. Implantable electrodes are invasive and require a pulse generator and power source, yet can precisely interface to a neural target. Noninvasive electrical stimulation requires no surgery, however the spatial precision of stimulation is low, and the depth of possible penetration limited to superficial targets. By using PV stimulator circuits, one can secure the precision and depth of a traditional implantable stimulator, yet with a simpler surgery and less bulky device which can be addressed from outside in a way analogous to noninvasive electrical stimulation. It can therefore be labeled as ‘minimally invasive’ during implantation, and ‘noninvasive’ during actual operation as a stimulator. Further, there are some unique

practical advantages to using noninvasive optical power transmission. The light source does not have to be in contact with the skin, nor does it have to be particularly close, due to the possibility of collimated light sources like laser diodes. A big advantage of having the optical stimulation from the point of view of electrophysiology experiments is the possibility to eliminate sources of electrical noise, as the light beam will not add any electrical noise. The only electrical artifact present will be the photogenerated stimulation pulse from the implanted PV, thus making recording easier, without complex filtered often required during noninvasive electrical stimulation. Overall, for any situation, animal or human, where space is limited and precludes implantation of bulky devices, a PV stimulator can be highly competitive.

As a wireless powering source for neuroelectronics, PVs present favorable opportunities, yet also impose unique design criteria. In this work, we have provided a range of practical parameters in terms of electrode size, material, and impedance, to facilitate

efficient design of light-powered wireless neurostimulators. Depending on the desired application, easily obtainable Si PVs or ultrathin and flexible OPVs may be optimal. In other cases, highly-efficient compound semiconductor devices may provide the best solution, despite their complexity relative to Si or organics. In this work, we have tested total currents and voltages using light illumination conditions which we assume to be practical based on our earlier research on *in vivo* PV neurostimulation, i.e. tens of mW cm^{-2} at a depth of roughly 1 cm of tissue, using 660 nm light [16]. However, light transmission is highly tissue-specific and experimental verification of the light intensities pertinent to the specific application with consideration of established safety and photothermal limits should be pursued. In general, PVs are a power source with a voltage limit dictated by the band gap of the semiconductor, and practically single-junction PVs absorbing red light will provide roughly up to 0.5 V. Therefore, when electrodes with high impedance are used, PVs must be connected in series to provide sufficient voltage. In the measurements we have presented, the two stimulation electrodes connected to the PV were always the same size, and therefore contribute equal impedance and charge injection capacity. It is important to note that if the two stimulation electrodes are different, the total delivered charge will always be limited by the electrode with the lowest charge injection capacity or highest impedance.

Our present work, built on demonstrations of direct PV neurostimulation over the past decade, describes the most minimalistic case of PVs directly driving neurostimulation electrodes. The advantage of such an approach is unparalleled simplicity. However, there are certain practical consequences and limitations. This minimalistic PV + stimulation ‘floating’ electrode arrangement does not enable feedback about the current being delivered. This means that practically, such PV stimulation could be used in cases where an easily quantifiable biomarker for stimulation exists that allows tracking of the stimulation effect. Examples include evoked motor activity, cardiovascular markers, downstream electrophysiological recording. All of these markers can be fed back to the optical light source delivering stimulation from outside. Therefore, a ‘closed loop’ kind of control is possible. Since the optical light source must be placed near the skin, we envision that PV stimulators would be appropriate for short and on-demand types of neuromodulation applications, rather than neuromodulation schemes which are running constantly. Another practical limitation is number of stimulation channels. To selectively activate a given photostimulation electrode, either the electrode sites must be far enough away from each other to limit cross illumination, or different band-gap semiconductors and/or

filters [36] must be used to allow wavelength tuning as a mode of control. Another promising strategy relies on semiconductor materials engineering. By choosing materials with intrinsically low lateral conductivity, it is possible to create monolithic devices which will only have active stimulation in the area that is illuminated, while the ‘dark’ parts of the device serve as a return electrode. This type of operation is possible with certain types of organic semiconductors [17], or with properly-tuned silicon [32]. While effective multielectrode operation is possible, practically achieving high-density stimulation arrays is a challenge. However, possibilities can be extended greatly if one considers PV as the mode of power transfer only, to power or recharge an implanted device with onboard electronics. This type of approach has been demonstrated for subdermal electronics and PV-rechargeable pacemakers [8, 33]. We believe that PV actuation of neurostimulator circuits presents an excellent experimental technique for free-moving animal experiments, where the small device size and easy implantation is a premium feature. Light can be delivered through small, wearable LED sources, via larger illumination of whole enclosures or smaller structures like tunnels/tubes (LEDs are cheap and efficient). Clinical applications will likely be indicated for neuromodulation therapies that are patient self-administered for several minutes per day, thus the patient can bring a handheld light source over their implant site to deliver stimulation in an on-demand fashion. The long-term efficacy and safety of PV power transfer approaches has yet to be demonstrated. We hope that the present work outlines actionable design principles so that neural engineers can fabricate devices appropriate to their given application.

Data availability statement

All data that support the findings of this study are included within the article (and any supplementary files).

Acknowledgments

This work has been supported by the European Research Council (ERC) under the European Union’s Horizon 2020 research and innovation program (E D G Grant Agreement No. 949191), by the Grant Agency of the Czech Republic under Contract 23-07432S. Sample fabrication was made possible by *CzechNanoLab* Research Infrastructure supported by MEYS CR (LM2023051). We thank Maciej Gryszel and Sven Ingebrandt for kindly providing PtO_x and IrO_x samples, respectively; and Aleksander Opančar for help with software for data analysis.

Author contributions

M J, D K, J G, and E D G conceived the project. M J fabricated the OPVs and performed all OPV measurements. O K and I G prepared the silicon PVs and measurement setup. M J, I G, and O K fabricated the electrode arrays of different stimulation materials. O K performed all measurements with Si PVs. M J and O K analyzed the data. M J prepared manuscript figures. E D G supervised the project. M J and E D G wrote the paper with input from all co-authors.

Conflict of interest

The authors declare no competing financial interests.

ORCID iDs

Imrich Gablech  <https://orcid.org/0000-0003-4218-1287>

Eric Daniel Głowacki  <https://orcid.org/0000-0002-0280-8017>

References

- [1] Krames E S, Peckham P H and Rezaei A R 2009 *Neuromodulation* (Academic)
- [2] Olofsson P S and Tracey K J 2017 Bioelectronic medicine: technology targeting molecular mechanisms for therapy *J. Intern. Med.* **282** 3–4
- [3] Birmingham K, Gradinaru V, Anikeeva P, Grill W M, Pikov V, McLaughlin B, Pasricha P, Weber D, Ludwig K and Famm K 2014 Bioelectronic medicines: a research roadmap *Nat. Rev. Drug Discov.* **13** 399–400
- [4] Chen R, Canales A and Anikeeva P 2017 Neural recording and modulation technologies *Nat. Rev. Mater.* **2** 1–16
- [5] Lee P M, Xiong Z and Ho J 2018 Methods for powering bioelectronic microdevices *Bioelectron. Med.* **1** 201–17
- [6] Thimot J and Shepard K L 2017 Bioelectronic devices: wirelessly powered implants *Nat. Biomed. Eng.* **1** 0051
- [7] Gutruf P et al 2018 Fully implantable optoelectronic systems for battery-free, multimodal operation in neuroscience research *Nat. Electron.* **1** 652–60
- [8] Kim J et al 2020 Active photonic wireless power transfer into live tissues *Proc. Natl Acad. Sci. USA* **117** 16856–63
- [9] Won S M, Cai L, Gutruf P and Rogers J A 2021 Wireless and battery-free technologies for neuroengineering *Nat. Biomed. Eng.* **7** 405–23
- [10] Blackmore J, Shrivastava S, Sallet J, Butler C R and Cleveland R O 2019 Ultrasound neuromodulation: a review of results, mechanisms and safety *Ultrasound Med. Biol.* **45** 1509–36
- [11] Piech D K, Johnson B C, Shen K, Ghanbari M M, Li K Y, Neely R M, Kay J E, Carmena J M, Maharbiz M M and Muller R 2020 A wireless millimetre-scale implantable neural stimulator with ultrasonically powered bidirectional communication *Nat. Biomed. Eng.* **4** 207–22
- [12] Singer A et al 2020 Magnetolectric materials for miniature, wireless neural stimulation at therapeutic frequencies *Neuron* **107** 631–43
- [13] Bashkatov A N, Genina E A, Kochubey V I and Tuchin V V 2005 Optical properties of human skin, subcutaneous and mucous tissues in the wavelength range from 400 to 2000 nm *J. Phys. D: Appl. Phys.* **38** 2543–55
- [14] Dąbrowski J M and Arnaut L G 2015 Photodynamic therapy (PDT) of cancer: from local to systemic treatment *Photochem. Photobiol. Sci.* **14** 1765–80
- [15] Abdo A, Sahin M, Freedman D S, Cevik E, Spuhler P S and Unlu M S 2011 Floating light-activated microelectrical stimulators tested in the rat spinal cord *J. Neural Eng.* **8** 056012
- [16] Ejneby M S et al 2022 Chronic electrical stimulation of peripheral nerves via deep-red light transduced by an implanted organic photocapacitor *Nat. Biomed. Eng.* **6** 741–53
- [17] Rand D, Jakešová M, Lubin G, Vebratė I, David-Pur M, Đerek V, Cramer T, Sariciftci N S, Hanein Y and Głowacki E D 2018 Direct electrical neurostimulation with organic pigment photocapacitors *Adv. Mater.* **30** 1707292
- [18] Paltrinieri T, Bondi L, Đerek V, Fraboni B, Głowacki E D and Cramer T 2021 Understanding photocapacitive and photofaradaic processes in organic semiconductor photoelectrodes for optobioelectronics *Adv. Funct. Mater.* **31** 2010116
- [19] Wang L et al 2012 Photovoltaic retinal prosthesis: implant fabrication and performance *J. Neural Eng.* **9** 046014
- [20] Ferlauto L et al 2018 Design and validation of a foldable and photovoltaic wide-field epiretinal prosthesis *Nat. Commun.* **9** 992
- [21] Wang B et al 2022 Electronic photoreceptors enable prosthetic visual acuity matching the natural resolution in rats *Nat. Commun.* **13** 6627
- [22] Palanker D, Vankov A, Huie P and Baccus S 2005 Design of a high-resolution optoelectronic retinal prosthesis *J. Neural Eng.* **2** S105–20
- [23] Mathieson K et al 2012 Photovoltaic retinal prosthesis with high pixel density *Nat. Photon.* **6** 391–7
- [24] Lemoine D, Simon E, Buc G and Deterre M 2020 In vitro reliability testing and in vivo lifespan estimation of wireless pixium vision PRIMA photovoltaic subretinal prostheses suggest prolonged durability and functionality in clinical practice *J. Neural Eng.* **17** 035005
- [25] Ghezzi D et al 2013 A polymer optoelectronic interface restores light sensitivity in blind rat retinas *Nat. Photon.* **7** 400–6
- [26] Missey F, Botzanowski B, Migliaccio L, Acerbo E, Głowacki E and Williamson A 2021 Organic electrolytic photocapacitors for stimulation of the mouse somatosensory cortex *J. Neural Eng.* **18** 066016
- [27] Zhang H et al 2019 Wireless, battery-free optoelectronic systems as subdermal implants for local tissue oximetry *Sci. Adv.* **5** eaaw0873
- [28] Haeberlin A et al 2015 The first batteryless, solar-powered cardiac pacemaker *Hear Rhythm* **12** 1317–23
- [29] Moon E, Blaauw D and Phillips J D 2017 Subcutaneous photovoltaic infrared energy harvesting for bio-implantable devices *IEEE Trans. Electron. Devices* **64** 2432–7
- [30] Donahue M, Ejneby M S, Jakesova M, Caravaca A S, Andersson G, Sahalianov I, Đerek V, Hult H, Olofsson P S and Głowacki E D 2022 Wireless optoelectronic devices for vagus nerve stimulation in mice *J. Neural Eng.* **19** 066031
- [31] Lu L et al 2018 Biodegradable monocrystalline silicon photovoltaic microcells as power supplies for transient biomedical implants *Adv. Energy Mater.* **8** 1–8
- [32] Li P et al 2024 Monolithic silicon for high spatiotemporal translational photostimulation *Nature* **626** 990–8
- [33] Song K et al 2016 Subdermal flexible solar cell arrays for powering medical electronic implants *Adv. Healthcare Mater.* **5** 1572–80
- [34] Jakešová M et al 2019 Optoelectronic control of single cells using organic photocapacitors *Sci. Adv.* **5** eaav5265
- [35] Abdo A and Sahin M 2011 Feasibility of neural stimulation with floating-light-activated microelectrical stimulators *IEEE Trans. Biomed. Circuits Syst.* **5** 179–88
- [36] Seymour E Ç, Freedman D S, Gökkaş M, Özbay E, Sahin M and Selim Ünlü M 2014 Improved selectivity from a wavelength addressable device for wireless stimulation of neural tissue *Front. Neuroeng.* **7** 1–12
- [37] Carvalho-de-Souza J L, Treger J S, Dang B, Kent S B H, Pepperberg D R and Bezanilla F 2015 Photosensitivity of

- neurons enabled by cell-targeted gold nanoparticles *Neuron* **86** 207–17
- [38] Acarón Ledesma H, Li X, Carvalho-de-Souza J L, Wei W, Bezanilla F and Tian B 2019 An atlas of nano-enabled neural interfaces *Nat. Nanotechnol.* **14** 645–57
- [39] Sytnyk M et al 2017 Cellular interfaces with hydrogen-bonded organic semiconductor hierarchical nanocrystals *Nat. Commun.* **8** 91
- [40] Aziz I A, Maver L, Giannasi C, Niada S, Brini A T and Antognazza M R 2020 Polythiophene-mediated light modulation of membrane potential and calcium signalling in human adipose-derived stem/stromal cells *J. Mater. Chem.* **1** 3777
- [41] Tortiglione C, Antognazza M R, Tino A, Bossio C, Marchesano V, Bauduin A, Zangoli M, Morata S V and Lanzani G 2017 Semiconducting polymers are light nanotransducers in eyeless animals *Sci. Adv.* **3** e1601699
- [42] Kozai T D Y and Vazquez A L 2015 Photoelectric artefact from optogenetics and imaging on microelectrodes and bioelectronics: new challenges and opportunities *J. Mater. Chem. B* **3** 4965–78
- [43] Stocking K C, Vazquez A L and Kozai T D Y 2019 Intracortical neural stimulation with untethered, ultrasmall carbon fiber electrodes mediated by the photoelectric effect *IEEE Trans. Biomed. Eng.* **66** 2402–12
- [44] Sherwood C P, Elkington D C, Dickinson M R, Belcher W J, Dastoor P C, Feron K, Brichta A M, Lim R and Griffith M J 2021 Organic semiconductors for optically triggered neural interfacing: the impact of device architecture in determining response magnitude and polarity *IEEE J. Sel. Top. Quantum Electron.* **27** 1–12
- [45] Chen K, Wu B, Krahe D, Vazquez A L, Siegenthaler J, Li W, Cui X T and Kozai T D 2024 Potential of photoelectric stimulation with ultrasmall carbon electrode on neural tissue: new directions in neuromodulation technology development *bioRxiv Preprint* (<https://doi.org/https://doi.org/10.1101/2024.02.17.580823>) (posted online 21 February 2024)
- [46] Jiang Y et al 2018 Rational design of silicon structures for optically controlled multiscale biointerfaces *Nat. Biomed. Eng.* **2** 508–21
- [47] Jiang Y, Parameswaran R, Li X, Carvalho-de-Souza J L, Gao X, Meng L, Bezanilla F, Shepherd G M G and Tian B 2019 Nongenetic optical neuromodulation with silicon-based materials *Nat. Protocols* **14** 1339–76
- [48] Zimmerman J F and Tian B 2018 Nongenetic optical methods for measuring and modulating neuronal response *ACS Nano* **12** 4086–95
- [49] Jiang Y and Tian B 2018 Inorganic semiconductor biointerfaces *Nat. Rev. Mater.* **3** 473–90
- [50] Derek V, Rand D, Migliaccio L, Hanein Y and Glowacki E D 2020 Untangling photofaradaic and photocapacitive effects in organic optoelectronic stimulation devices *Front. Bioeng. Biotechnol.* **8** 284
- [51] Shockley W and Queisser H J 1961 Detailed balance limit of efficiency of p-n junction solar cells *J. Appl. Phys.* **32** 510
- [52] Dennler G, Scharber M C and Brabec C J 2009 Polymer-fullerene bulk-heterojunction solar cells *Adv. Mater.* **21** 1323–38
- [53] Tang C W 1986 Two-layer organic photovoltaic cell *Appl. Phys. Lett.* **48** 183–5
- [54] Gryszel M, Markov A, Vagin M and Glowacki E D 2018 Organic heterojunction photocathodes for optimized photoelectrochemical hydrogen peroxide production *J. Mater. Chem. A* **6** 24709–16
- [55] Gablech I, Migliaccio L, Brodský J, Havlíček M, Podešva P, Hrdý R, Ehlich J, Gryszel M and Glowacki E D 2023 High-conductivity stoichiometric titanium nitride for bioelectronics *Adv. Electron. Mater.* **9** 2200980
- [56] Gryszel M, Jakešová M, Lednický T and Glowacki E D 2022 High-capacitance nanoporous noble metal thin films via reduction of sputtered metal oxides *Adv. Mater. Interfaces* **2022** 2101973
- [57] Bromm B and Lullies H 1966 Über den Mechanismus der Reizwirkung mittelfrequenter Wechselströme auf die Nervenmembran *Pflugers Arch. Gesamte Physiol. Menschen Tiere* **289** 215–26
- [58] Schoen I and Fromherz P 2008 Extracellular stimulation of mammalian neurons through repetitive activation of Na⁺ channels by weak capacitive currents on a silicon chip *J. Neurophysiol.* **100** 346–57